

# Effects of Surface Roughness on Shock-Wave/Boundary-Layer Interaction using a Hollow Flare Cylinder Model

Matt Garcia<sup>1</sup> and Christopher S. Combs<sup>2</sup>

*The University of Texas at San Antonio, San Antonio, Texas, 78249, USA*

Shock-wave/boundary-layer interactions have been a subject of importance and research interest for several decades now as various high-speed systems encounter this phenomenon during operation. These interactions occur when a shock-wave impinges upon the boundary layer of a flight vehicle and could potentially lead to the detachment of the boundary layer from the vehicle's surface. This phenomenon could also cause disturbances within the flow and initiate the unstart of an engine or induce serious damage to components and airframes. Studies have shown how various physical properties such as surface roughness can influence boundary layer development and state. However, more research is needed to understand the interaction between surface roughness and shock-wave/boundary-layer interactions. This testing campaign was conducted at the University of Tennessee Space Institute to assess the effects of surface roughness on shock-wave/boundary-layer interactions utilizing a hollow cylinder flare model. Image results from this campaign were acquired using high-speed schlieren imaging collected at a frame rate of 200 kHz within a Mach 4 flow of this facility at a Reynolds number of  $21 \times 10^6 \text{ m}^{-1}$ . The separation shock foot from the shock-wave/boundary-layer interactions of the hollow cylinder flare was tracked by analyzing the schlieren images with the use of a shock tracking algorithm. The algorithm permits the user to account for wind tunnel movement by repositioning images and tracking the time history of the shock foot position. Methods such as applied statistics, spectral analysis, intermittency, and zero-crossing frequencies were used to understand the effects of surface roughness on the unsteadiness within the investigated interactions.

## Nomenclature

$f$	=	<i>frequency</i>
$f_c$	=	<i>shock zero-crossing frequency</i>
$G$	=	<i>one-sided autospectral-density function</i>
$L_s$	=	<i>shock-location</i>
$L_{\bar{s}}$	=	<i>mean shock-location</i>
$P(X)$	=	<i>probability density function</i>
$R_a$	=	<i>average roughness</i>
$x$	=	<i>streamwise distance</i>
$\bar{x}$	=	<i>mean</i>
$y$	=	<i>normal distance from the wall</i>
$\gamma_{xy}^2$	=	<i>coherence</i>
$\gamma_{L_s}$	=	<i>intermittency</i>
$\delta$	=	<i>boundary layer thickness</i>
$\rho$	=	<i>correlation</i>
$\sigma$	=	<i>standard deviation</i>
$\sigma^2$	=	<i>variance</i>

---

<sup>1</sup> Graduate Research Assistant, Department of Mechanical Engineering, AIAA Student Member.

<sup>2</sup> Dee Howard Endowed Assistant Professor, Department of Mechanical Engineering, AIAA Senior Member.

## I. Introduction

**S**UPERSONIC and hypersonic flows produce high enthalpy conditions along the surface of aircrafts, which in consequence lead to the ablation of the outer layer surface.[1] This process is known to alter the shape of the affected surface and produce non-uniform surface roughness, striations, or cross-hatching.[2] In addition to the surface roughness variant during flight, airflow travels throughout geometries such as cylinders and ramps which cause shock-wave/boundary-layer interactions (SWBLI) to occur.[3] This phenomenon is seen to occur on the surfaces of pylons, Pitot probes, and contours within engines. Changes in surface roughness and SWBLIs can be a crippling occurrence which leads to altered fluid dynamics and aircraft damage.[4]

The effects of surface roughness within supersonic and hypersonic flows have been investigated to analyze the affected boundary layer structure.[1, 5, 6] Testing various surface roughness can provide insight for how the Reynolds shear stress changes with respect to roughness[6] and approximate boundary layer velocity profiles biased on roughness height.[1] Wall roughness studies provide a foundation for categorizing the effects of surface roughness, however not all aircraft surfaces are orthogonal to the flow. To follow through with these studies, changing the geometry of the surface can provide another layer of flow characterization and produce effects such as SWBLIs.

Studies on SWBLI have been analyzed within impinging shocks[7], cylinders[8] and ramp[9] geometries to better understand and classify shock structure occurrences. Unique frequency spectra has been found and associated with different kinds/types of SWBLI and have been typically obtained through the power spectra of high-speed schlieren images while using applied statistics on the structures developed within the interaction.[10] Structures such as separation shocks can be visualized and easily identified with schlieren imaging. However, location tracking of separation shocks is a difficult task when tens-of-thousands of images are being analyzed. The use of shock tracking scripts can be implemented to ease the laborious process[11], and yield faster results when compared to manual rendering solutions.

Such a script has been developed and used for this experimental test campaign to track the position of the shock foot immitted from the separation shock. The separation shock is induced by a hollow cylinder flare model while a change in surface roughness will be implemented to explore its effects of the SWBLI. The proceeding text will compare these effects occurring on a smooth (bare HCF model) to those of a rough (carbon fiber on HCF model) surface.

## II. Experimental Program

### A. Wind Tunnel Facility

The Mach 4 Ludwig Tube facility at the University of Tennessee Space Institute (UTSI) was used to acquire qualitative schlieren data for these experiments. This wind tunnel has a test section volume of  $610 \times 610 \times 1830$  mm ( $24 \times 24 \times 72$  in). The unheated heated air provided by the driver tube is triggered by a series of Mylar diaphragms, resulting in a freestream Mach number of 4 with a Reynolds number range of  $3.04 - 50.3 \times 10^5/\text{m}$  ( $1.0 - 16.5 \times 10^6/\text{ft}$ ). The vacuum tank can evacuate  $31 \text{ m}^3$  (8200 gal) of air down to 130Pa (1 Torr). Optical windows with a viewing area of  $280 \times 432\text{mm}$  ( $11 \times 17$  in) are located on the test section side walls.[12]

### B. Model Geometries

A hollow cylinder flare model (HCF), as shown in Fig. 1, was used in this test campaign with a  $30^\circ$  aluminum flare and an adjustable steel body placed at a length of 320 mm (12.6 in), respectively. The hollow cylinder flare model was mounted to the bottom test section plate by the means of a sting. The steel body of the HCF was cleaned thoroughly to maintain a polished surface for the smooth surface test, while 30K carbon fiber was applied to the steel body of the HCF with a spray-on adhesive. The leading edge of the carbon fiber was secured with masking tape to prevent fraying when handling the model. The surface roughness average values of  $R_a = 0.85$  and  $9.22 \text{ um}$  were determined using a profilometer after preparing the surface both surfaces. A HCF model was used as it was readily available and the conventional Z-type schlieren optical setup was able to capture a path integrated cross-section of the 3-D SWBLI.

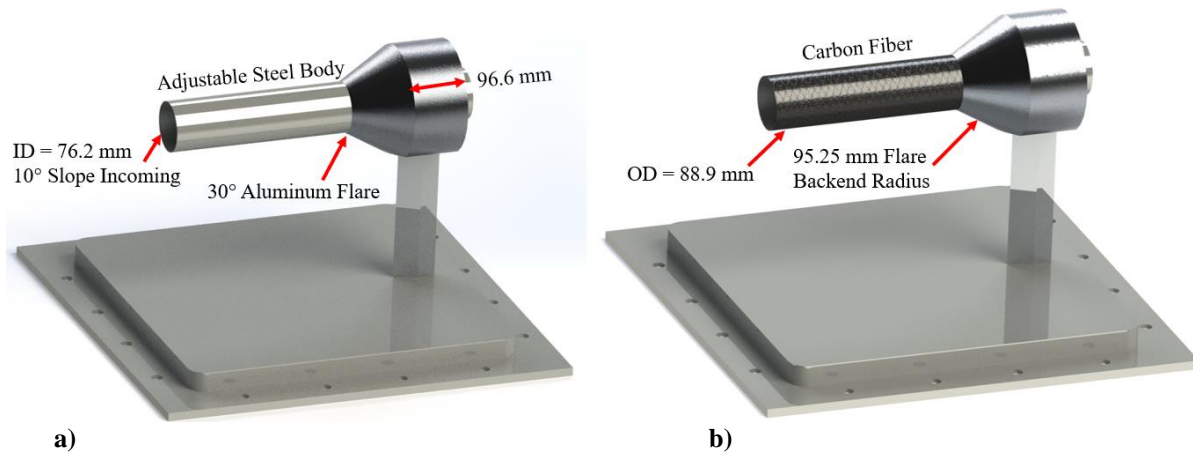


**Fig. 1. Dimensional schematics of hollow cylinder flare model, a) smooth surface, and b) rough surface.**

**C. Schlieren Experimental Setup**

Schlieren images were collected to acquire time and spatially-resolved shock position. The schlieren system was configured using a Z-type optical setup with 2.54-m-focal-length mirrors, using a Photron FASTCAM SAZ high-speed camera fitted with the camera attachments shown in Table 1. The image resolution differed from the smooth and rough surface tests as the rough SWBLI was larger in size compared with the smooth test trial. A high-powered, Luminus pulsed light-emitting diode provided high-intensity pulsed light at 200 kHz fast enough to freeze the motion of the shock structures within each image.

**Table 1. Image properties**

Surface	Image Resolution	Acquisition Rate	Scale	Camera Attachments
Smooth	640 × 122 pixels	200 kHz	10.95 pixel/mm	300 mm lens + 2x teleconverter
Rough	384 × 176 pixels	200 kHz	2.19 pixel/mm	70-200 mm lens

**D. Image Processing**

Schlieren images were imported into a custom MATLAB® script to correct the placement of images and determine the shock-location,  $L_s$ , of the SWBLI.[11] To ensure accurate shock tracking, a reference point was established at the intersection of the HCF body and flare. However, the wind tunnel’s vertical and horizontal movement throughout the test run varied the position of the reference point. The wind tunnel motion was corrected by a 2-D cross-correlation of the image stacks with the reference image. The pixel adjustment distance for each image was determined via lag values obtained within the 2-D cross-correlation. The maximum peak correlation amplitude in both axes were found and matched with the lag value. The lag values determine the required pixel shift needed to match the location of the reference image in the vertical and horizontal directions. The shock wave was identified by setting a pixel intensity threshold within a predetermined window size. The location of pixel values that agree with the threshold criteria were linearly interpolated to produce the images shown in below. Most instantaneous images do not have a shock wave that extends to the HCF surface. Therefore, such a script is needed to identify the  $L_s$ . Figure 2 shows an image sequence of computed shock positions acquired by the shock tracking portion of the script. The use of this script also reduces the amount of time used to identify the shock position within large image sets. Frequency spectra of the processed data were computed using the MATLAB® pwelch command with a fast Fourier transform size of 7000 points and a Hamming window with 50% overlap.

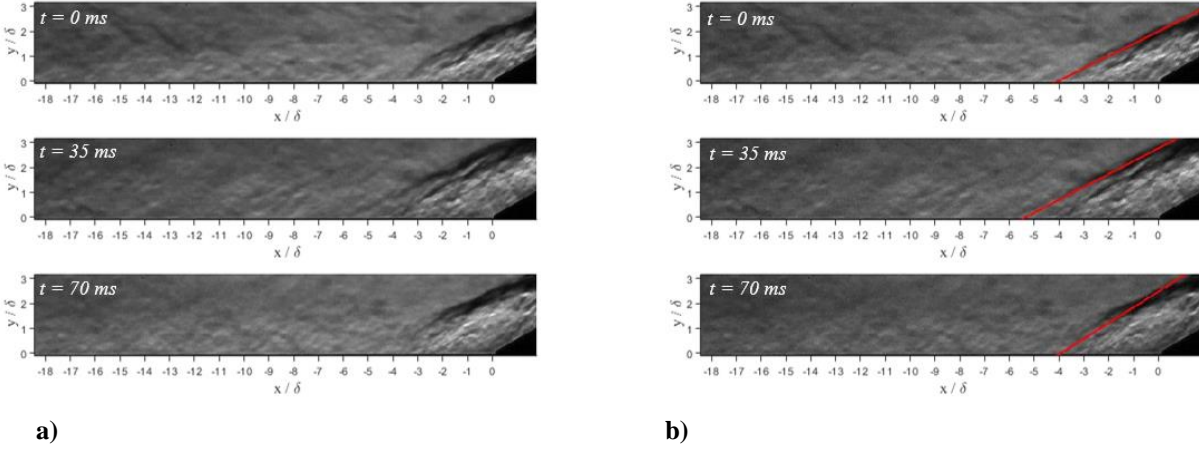


**Fig. 2. Representative schlieren image sequence demonstrating computed shock positions of smooth surface, a) instantaneous images, and b) shock tracking images**

Placement of the shock tracking window and the selection of threshold pixel-intensities should be selected properly by noting the structures created by SWBLIs shown in Fig. 3. The shockwave has noticeably strong density gradients than the rest of the flow due to the knife-edge’s horizontal placement. A low pixel intensity value can be selected for the threshold due to this phenomenon. However, placing the shock detection region over the flare, may cause the script to detect low pixel intensity values within the flare region while producing inaccurate shock tracking. Software such as ImageJ can be used to pinpoint pixel intensities to determine a low and high pixel intensity threshold. In some cases, the pixel intensity threshold may need to vary throughout the image set to accurately detect the shock structure. Unwanted outlying shock locations can be discarded after image processing. Notably, best practice suggests optimizing the shock tracking window and threshold before filtering outliers within data sets.

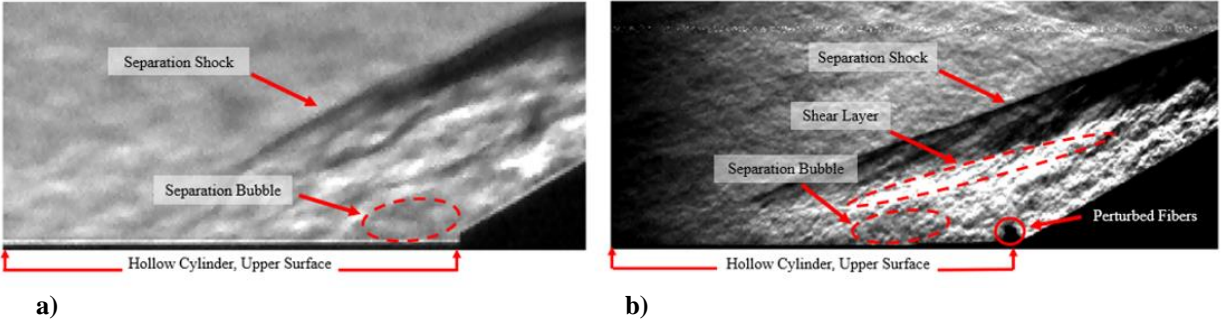


**Fig. 3. Annotated schlieren diagram, a) smooth surface, and b) rough surface**

**III. Results and Discussion**

Instantaneous and mean images of the two surfaces can be seen in Fig. 4. The instantaneous images show that the boundary layer is turbulent due to the structures present within the flow. The mean images can be used to locate the mean shock location,  $L_{\bar{s}}$ , by tracing the upper part of the shockwave down to the surface of the HFC. The  $L_{\bar{s}}$  for the smooth surface can be estimated to lie close to  $-5 x/\delta$ , while the rough surface’s  $L_{\bar{s}}$  is out of frame while likely lying between  $-6$  and  $-7 x/\delta$ . The noticeable circular structure on top of the shock wave, within the smooth surface run, is due to a dust particle on the window, while the rough surface run has a horizontal line with high pixel intensities due to damage within the camera’s sensor. These disturbances within the images can be ignored as they do not contribute to the SWBLI.

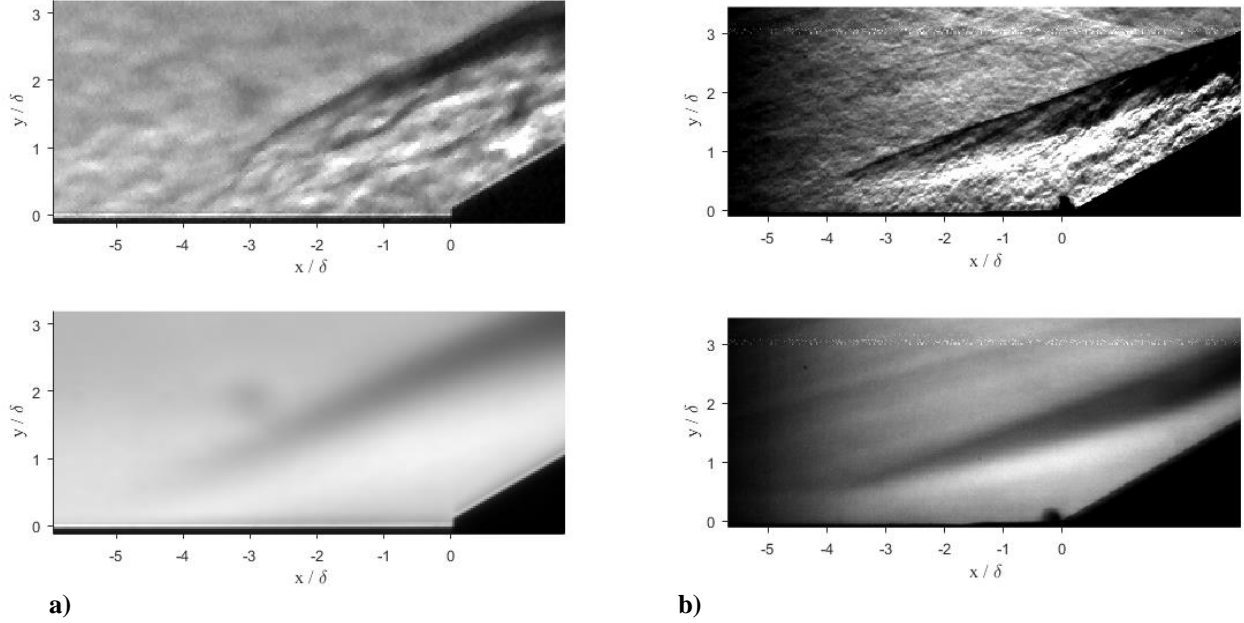


**Fig. 4. Instantaneous (top) and mean (bottom) schlieren visualizations of SWBLI, a) smooth surface, and b) rough surface**

The pixel-intensity standard deviation (rms) fields for the smooth and rough surfaces are shown in Fig. 5. The *light-colored* sections within the SWBLI indicate a high deviation of pixel-intensity with respect the mean pixel-intensity, respectively. As the shockwave approaches the surface of the HCF, the deviation begins to lessen. At this point, the boundary layer thickness was estimated to be  $\delta = 2.6$  and  $20$  mm for the smooth and rough case, respectively. The boundary layer thickness was used as a normalization factor to the scaling images. The *one point* in the vertical axis indicates the boundary layer height approximation within the figures. The boundary layer height grew by a factor of 7 due to an increased surface roughness 10 times greater than the smooth test trial.

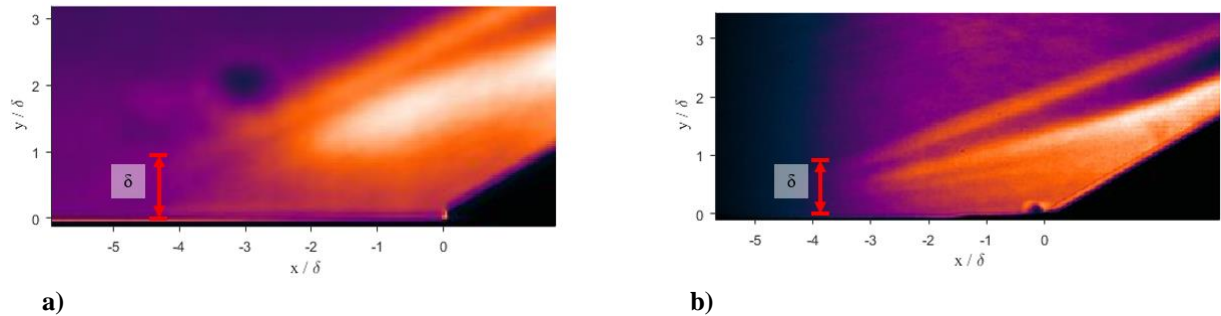


**Fig. 5. RMS fields for SWBLI, a) smooth surface, and b) rough surface**

The normalized  $L_s$  was tracked through time shown in Fig. 6a. The shock foot position data was filtered with a moving mean of 50 data points while data that was three standard deviations away from the mean was removed then linearly interpolated. The rough surface data set produces less noise with respect to the smooth data set, as the rough surface test trial produced a larger shockwave for the script to detect. An increase in shockwave size allows the script to locate more points that lie between the pixel-intensity threshold and yield a less noisy data set. The probability density function,  $P(X)$ , provided in Fig. 6b, confirms that the  $L_s$  lies on  $-5.07$  and  $-7.96$   $x/\delta$  for the smooth and rough surface tests, respectively. A summary of the shock-motion is provided within Table 2 along with statistical moments and unsteadiness.

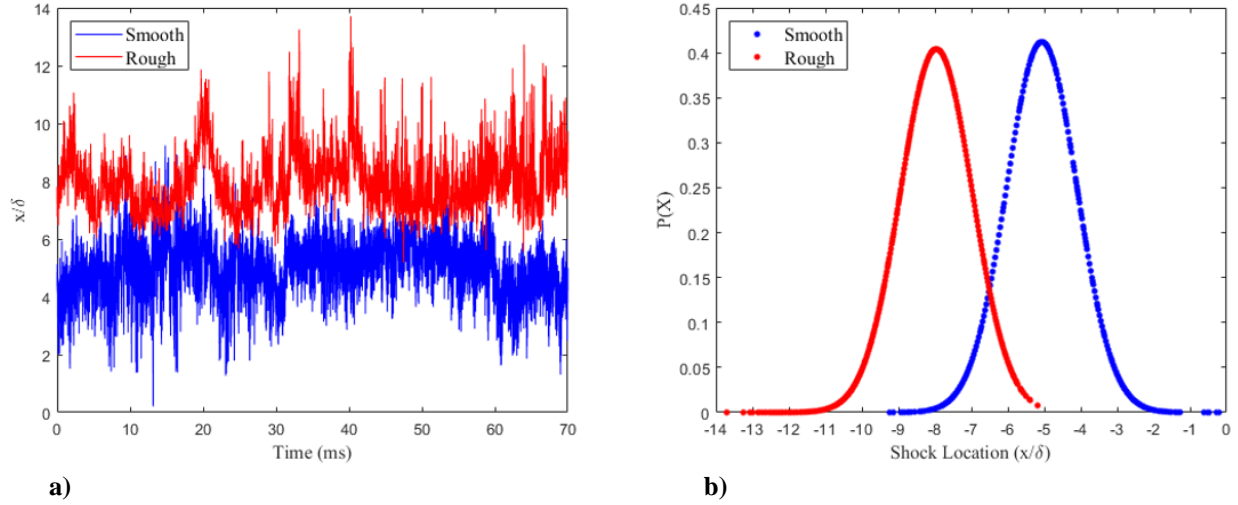


**Fig. 6. a) Normalized time history, and b) PDF of smooth and rough SWBLI**

**Table 2. Summary of shock-motion**

Surface	$R_a$ (um)	$\delta$ (mm)	$L_{\bar{s}}$ ( $x/\delta$ )	$\sigma$	$\sigma^2$	Kurtosis	Skewness	$\sigma^2/\bar{x}$
Smooth	0.85	2.6	5.07	0.97	0.94	3.7	-0.38	0.184
Rough	9.22	20	7.96	0.99	0.97	4.4	0.92	0.122

The spectral signature of the shock motion is shown in Fig. 7a to further investigate the effects of surface roughness within the SWBLI. The spectral energy of the signals differ from each other while both signals demonstrate spectral fluctuations after the intersection frequency at 15 kHz. This fluctuation is indicative of a variance within turbulent structures. The coherence,  $\gamma_{xy}^2$ , plot in Fig. 7b confirms that the signals do not possess similar spectral energies due to a low value of  $\gamma_{xy}^2$  and high fluctuation at high frequencies.

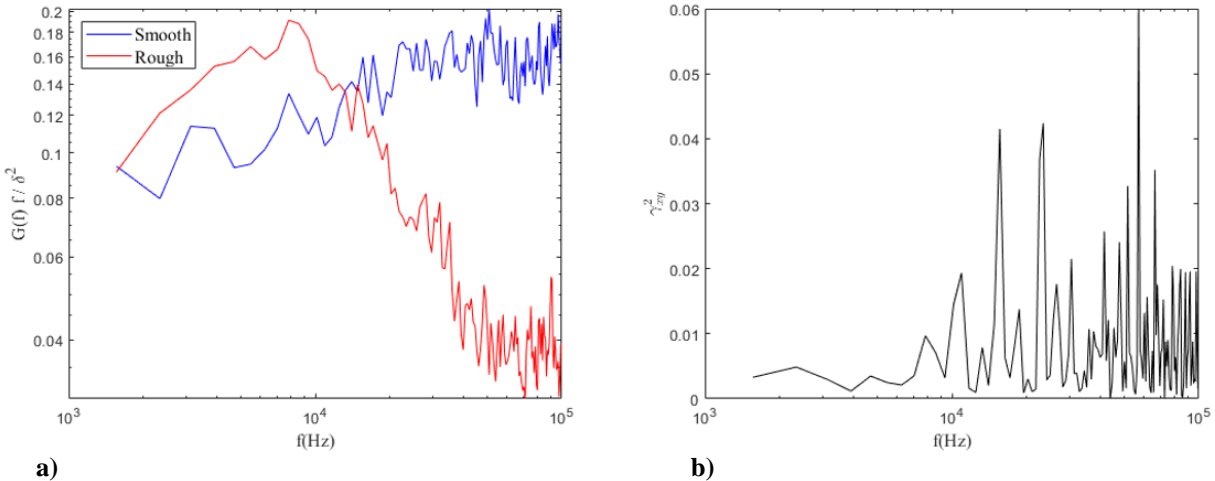


**Fig. 7. a) Power spectra of the shock position unsteadiness for smooth and rough surface, and b) coherence for rough and smooth surface.**

Another form to interpret the shock-location data is by the intermittency,  $\gamma_{L_s}$ . The percentage of time that the shock is upstream of a given location is shown in Fig. 8a. The shock foot placement of the rough surface is 100% of

the time past the location  $-6 x/\delta$ , while the shock foot placement of the smooth surface is 100% of the time upstream of  $-2 x/\delta$ . Both cases show a decline in  $\gamma_{L_s}$  as the shock foot passes the  $L_s$ . Figure 8b shows the zero-crossing frequency,  $f_c$ , of the  $L_s$  as a frequency when the shock travels a given  $x/\delta$  location. The  $f_c$  shows that the transitional interaction of both data sets has a magnitude of  $9 x/\delta$  while the rough surface's interaction is shifted  $4 x/\delta$  upstream of the smooth surface's interaction, respectively. The peak  $f_c$  for the smooth and rough case lie at  $5$  and  $8 x/\delta$  upstream of the ramp with a magnitude of  $30$  and  $15$  kHz.

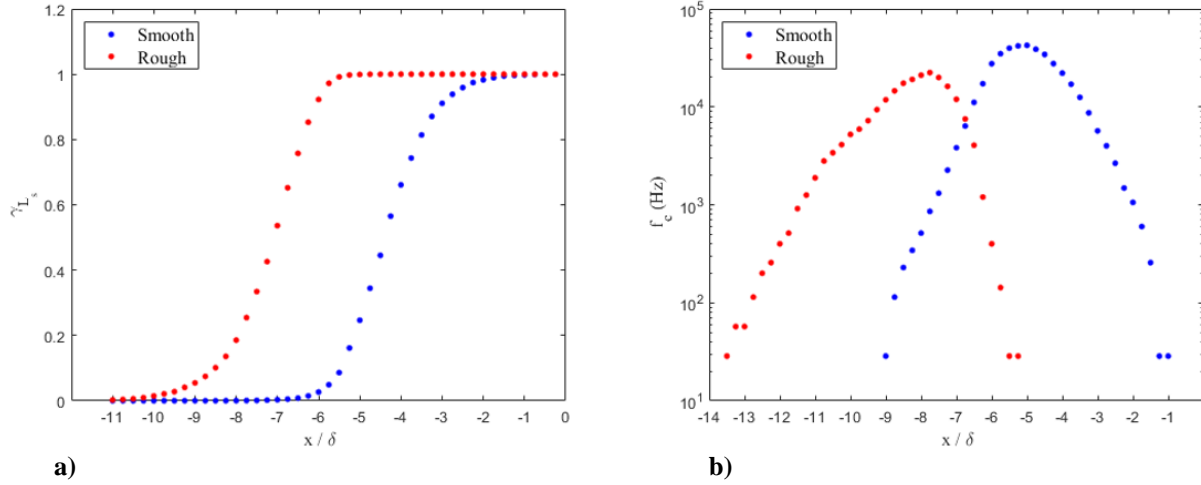


**Fig. 8 a) Intermittency of the rough and smooth surfaces'  $L_s$ , and b) zero-crossing frequency for smooth and rough surfaces'  $L_s$ .**

#### IV. Conclusion

An experimental study on the effects of surface roughness within a shock-wave/boundary-layer interaction (SWLBI) at the Mach 4 Ludwig Tube facility in University of Tennessee Space Institute (UTSI) was performed. Schlieren imaging of the two surfaces was obtained to analyze the unsteadiness of the SWBLI. The instantaneous and mean images of the two surfaces provide an approximation for the shock location,  $L_s$ . The mean shock location,  $L_s$ , was confirmed by the probability density function to lie on  $-5.07$  and  $-7.96 x/\delta$  for the smooth and rough surface tests, respectively. The spectral energy analysis suggests that both signals vary spectrally from each other while demonstrating a high spectral fluctuation after 15 kHz. The shock foot intermittency,  $\gamma_{L_s}$ , of the smooth and rough surfaces were 100% of the time past the location  $-2$  and  $-6 x/\delta$  suggesting that the lifetime of the shock wave will live upstream of these two points, while the zero-crossing frequency,  $f_c$ , showed that the transitional interaction of both data sets has a magnitude of  $9 x/\delta$  while the rough surface's interaction is shifted  $4 x/\delta$  upstream of the smooth surface's interaction. There are noticeable distinctions and similarities between the two surfaces provided throughout this analysis, yet a larger range of surface roughness are needed to categorize the effects of surface roughness on SWBLI.

#### Acknowledgments

This material is based upon work supported by the Air Force Office of Scientific Research under award number FA9550-20-1-0190 and by the U. S. Office of Naval Research under award number N00014-15-1-2269. Additional support was also provided by NASA grant number 80NSSC19M0194. The authors would like to acknowledge Dr. John Schmissuer, Dr. Mark Gragston, Dr. Cary Dean, and Mason Pohlman for their assistance and access to the UTSI Mach 4 facility for this experimental campaign. The authors would like to further acknowledge Eugene Hoffman and Jose Rodriguez for the acquisition of the data analyzed in this manuscript.

#### References

- [1] S. Dipankar, S. Alexander, and P. Michael, "PIV Experiments on a Rough Wall Hypersonic Turbulent Boundary Layer," ed.

- [2] D. E. Berg, "Surface Roughness Effects on the Hypersonic Turbulent Boundary Layer," ProQuest Dissertations Publishing, 1977.
- [3] D. V. Gaitonde, "Progress in shock wave/boundary layer interactions," *Progress in aerospace sciences*, vol. 72, pp. 80-99, 2015, doi: 10.1016/j.paerosci.2014.09.002.
- [4] E. N. A. Hoffman *et al.*, "Modal Analysis of Cylinder-Induced Transitional Shock-Wave/Boundary-Layer Interaction Unsteadiness," *AIAA journal*, pp. 1-19, 2021, doi: 10.2514/1.J060880.
- [5] R. M. Latin and R. D. W. Bowersox, "Flow Properties of a Supersonic Turbulent Boundary Layer with Wall Roughness," *AIAA journal*, vol. 38, no. 10, pp. 1804-1821, 2000, doi: 10.2514/2.862.
- [6] D. K. Brian, S. C. Christopher, A. K. Phillip, D. S. John, and J. P. Scott, "Investigation of the Effects of Distributed Surface Roughness on Supersonic Flows," ed.
- [7] D. Estruch, D. G. MacManus, D. P. Richardson, N. J. Lawson, K. P. Garry, and J. L. Stollery, "Experimental study of unsteadiness in supersonic shock-wave/turbulent boundary-layer interactions with separation," *Aeronautical journal*, vol. 114, no. 1155, pp. 299-308, 2010, doi: 10.1017/S0001924000003742.
- [8] C. S. Combs, E. L. Lash, P. A. Kreth, and J. D. Schmisser, "Investigating Unsteady Dynamics of Cylinder-Induced Shock-Wave/Transitional Boundary-Layer Interactions," *AIAA journal*, vol. 56, no. 4, pp. 1588-1599, 2018, doi: 10.2514/1.J056553.
- [9] N. T. Clemens and V. Narayanaswamy, "Low-Frequency Unsteadiness of Shock Wave Turbulent Boundary Layer Interactions," *Annual review of fluid mechanics*, vol. 46, no. 1, pp. 469-492, 2014, doi: 10.1146/annurev-fluid-010313-141346.
- [10] C. S. Combs, J. D. Schmisser, B. F. Bathel, and S. B. Jones, "Unsteady Analysis of Shock-Wave/Boundary-Layer Interaction Experiments at Mach 4.2," *AIAA journal*, vol. 57, no. 11, pp. 4715-4724, 2019, doi: 10.2514/1.J058073.
- [11] C. S. Combs, P. A. Kreth, J. D. Schmisser, and E. L. Lash, "Image-Based Analysis of Shock-Wave/Boundary-Layer Interaction Unsteadiness," *AIAA journal*, vol. 56, no. 3, pp. 1288-1293, 2018, doi: 10.2514/1.J056390.
- [12] A. K. Phillip, G. Mark, D. Kirk, and D. S. John, "Design and Initial Characterization of the UTSI Mach 4 Ludwig Tube."